Insight on the generation of near infra-red (NIR) absorbing species in electrochromic Surface-Anchored Metal-Organic Frameworks

Antoine Mazel, Matteo Fornasarig, Josianne Owona, Lionel Truflandier, Frédéric Castet, Aline Rougier

ARTICLE

Insight on the generation of near infra-red (NIR) absorbing species in electrochromic Surface-Anchored Metal-Organic Frameworks.

Received 00th January 20xx,
Accepted 00th January 20xx

DOI: 10.1039/x0xx00000x

Antoine Mazel[*a], Matteo Fornasarig[b], Josianne Owona[b,c], Lionel Truflandier[b], Frédéric Castet[b] and Aline Rougier[*a]

Due to their verstaility and easy processing, Surface-Anchored Metal-Organic Frameworks (SurMOFs) have received recent interest as promising electrochromic thin films. Herein a step forward in their use and characterization was achieved thanks to the integration of $\{Zn_2(PDICl_4)_2\}$ SurMOFs in a multi-layer electrochromic device (ECD), based on membrane-like electrolyte. Optical and electrochemical properties of the ECD were fully characterized, revealing a two-step reduction process localized on the organic ligand and involving subsequent near infra-red (NIR) and cyan absorbing states, leading to optical modulation of the films. The species responsible for this absorption were isolated and identified in the reduced states. In parallel to experimental characterization, quantum chemistry was successfully used to investigate the structure-properties relationship of the SurMOF revealing additional information regarding the structure and the local environment of the electrochromic ligand.

1. Introduction

Electrochromism (EC) refers to a change of the optical properties of a material upon application of a voltage[1]. In the case of organic-based EC materials, this optical modulation comes from the electrochemically generated radicals[2]. Some organic molecules can undergo several reduction processes, yielding different radicals with their own absorption properties. Usually, electrochromic active organic materials come under the form of polymers deposited on transparent conductive oxide (TCO)[3,4]. One of the limitations of this strategy lies in the amount of monomers needed to generate the EC polymer, thus preventing the use of highly sophisticated molecules, usually obtained in multi-step fashion. In addition, the lack of control over the repartition of the organic active sites may prevent in-depth study.

Hybrid materials such as Metal-Organic Frameworks (MOFs) are synthesized via self-assembly of the organic ligands and metallic nodes and are thus ideal candidates to create functional materials where the properties can arise from the organic ligand. Direct growth of ligands and metallic nodes over FTO/glass substrates yielded the first EC MOFs thin films[5,6].

More recently, a strategy based on the sequential and controlled immobilization key component of the MOFs lead to the fabrication of highly homogenous hybrid materials where constituents present a preferential orientation with controlled relative positions. These crystalline hybrid thin films are called Surface-Anchored Metal-Organic Frameworks (SurMOFs)[7,8]. This method uses a very small amount of precursors (few mg/cm²) making SurMOFs ideal candidates for the integration of highly sophisticated ligands into functional materials.

Because of their hybrid nature, electrochromic properties of SurMOFs can arise from the metallic node, the organic linker or both. Recently, EC SurMOFs, in which perylene diimide (PDI) linkers were responsible of the optical modulation, were reported[9]. $\{Zn_2(PDICl_4)_2\}$ materials exhibit an unexpected behaviour with two different colours generated depending on the nature of the electrolyte. Interestingly, in addition of a blue colour linked to lithium insertion, reduction in pure EMITFSI (1-ethyl-3-methylimidazolium bis-(trifluoromethanesulfonyl)-imide) led to a cyan colour attributed to the formation of radicals. Because of the lack of stability in this electrolyte, further characterizations could not be performed on single layers.

In this work, prototype devices using the $\{Zn_2(PDICl_4)_2\}$ SurMOF structure were built by sandwiching EMITFSI electrolyte between Indium Tin Oxide (ITO)/glass substrate and SurMOF@ITO/glass. Thanks to this configuration, stability in this electrolyte was greatly improved and additional characterizations were performed on the electrochromic behaviour of the SurMOF. More specifically, absorption spectroscopy revealed the stabilization and formation of the mono radical by reduction of the $PDICl_4$ linker. Interestingly, this species was formed with a very small potential leading to the efficient generation of a near infra-red absorbing state, starting from an orange initial state. In addition, *in-situ* spectroelectrochemistry analysis gave insight on the formation of the mono and bi radical species. This work opens up new possibility for the design of NIR-based electrochromic materials

[a.] *Univ. Bordeaux, CNRS, Bx INP, ICMCB, UMR 5026, F-33600 Pessac, France*
[b.] *Univ. Bordeaux, CNRS, Bx INP, ISM, UMR 5255, F-33405 Cedex Talence, France*
[c.] *Donostia International Physics Center (DIPC), Manuel Lardizabal Ibilbidea 4, 20018 Donostia, Euskadi, Spain*

Electronic Supplementary Information (ESI) available: [details of any supplementary information available should be included here]. See DOI: 10.1039/x0xx00000x

that are of huge interest, especially for their heat-absorbing capacity[10].

Thanks to the highly ordered structure of SurMOFs, computational chemistry techniques can also be exploited to gain deeper understanding of structure-property relationships in these materials[11,12]. Herein the structural, optical and electrochromic properties were investigated by combining quantum chemistry methods with experimental analysis. This strategy provided insights on the local environment of the ligands, as well as on the absorbing electronic states at different stages of the electrochromic process.

2. Experimental

2.1 Materials and method

All the SurMOFs synthesis, optical and electrochemical characterizations were performed at room temperature in air. Ethanol, DMF and Zinc acetate were purchased from Aldrich and used without further purification. EMITFSI in PMMA/butanone (60:40 wt.%) were purchased from Solvionics. ITO/glass substrates with a resistance of 30 Ω/sq were purchased from Solems.

2.1.1 Preparation of the $\{Zn_2(PDICl_4)_2\}$ SurMOFs

All the SurMOFs were fabricated by spray technique in a layer-by layer fashion on pre-cleaned ITO/glass substrate. The substrates were cleaned by ultrasonic treatment in ethanol/water (1:1) bath for 30 min, then treated by activation by UV/O_2 to remove impurities and generate a surface with hydroxyl groups. 1 mM zinc acetate ethanolic solution and 20 µM of $PDICl_4$ solutions (5% DMF + 95 % Ethanol) were sequentially deposited onto the substrates for 15s and 25s in a layer-by-layer fashion using nebulization nozzles. After waiting for 35s to enable further coordination, the samples were rinsed with ethanol to remove unreacted or by-products from the surface. The thickness of the samples was controlled by the number of deposition cycles. Every SurMOFs were made with a 30 cycles process, requiring 200mL of $PDICl_4$ and 150mL of $Zn(OAc)_2$ solutions. The thickness of the films was estimated to be 450nm, according to previous paper [9].

2.1.2 X-Ray Diffraction (XRD)

X-ray diffraction measurements were carried out using a PANalytical X'pert PRO MPD with Bragg-Brentano ϑ-2ϑ geometry equipped with a secondary monochromator (KαCu =1.5418 Å) and an X'Celerator detector over an angular range of 2ϑ = 3-20°.

2.1.3 Device preparation

On pre-cleaned ITO/glass substrate EMITFSI in PMMA/butanone (60:40 wt.%) was spread on the ITO side and placed under vacuum for 5min to remove air bubbles. The ITO substrate covered with electrolyte was heated at 80°C for 5min and the SurMOF thin film was placed onto the sticky electrolyte membrane. A weight was applied over the device to ensure good contact, after 15min the weight was removed and the device was ready to be used.

2.1.4 Electrochemical and optical measurements

Electrochemical measurements were carried out in a device configuration using a BioLogic SP50 potentiostat/galvanostat apparatus with SurMOF on ITO/glass as the working electrode and ITO/glass as the counter electrode. The operating voltage was controlled between [-4 V,1 V] in EMITFSI, a salt-free electrolyte. Regarding the optical properties of the device, absorbance of the SurMOF was measured *in-situ* using a Varian Cary 5000 UV-Vis-NIR spectrophotometer coupled with a BioLogic SP50 potentiostat/galvanostat apparatus in the same device configuration as electrochemical measurements. Home-made 3D printed sample holder was used to record the optical properties of the device.

2.1.5 Quantum chemistry method

The crystal structure geometry was optimized by using density functional theory (DFT) with periodic boundary conditions (PBC), as implemented in the Conquest software[13–15] based on norm-conserving pseudopotentials (NCPP) using Hamann's version[16] and numerical atomic orbitals[17]. The size of the valence shell for the NCPP were standard for p-block atoms whereas, for Zn, the 3s and 3p semi-core states were included in valence. The quality of the basis was double-zeta + polarization functions. The exchange correlation functional was PBE including Grimme dispersion corrections (D2 version15). To minimize PBC constraints, a supercell of 8 metallic cores (containing each 2 Zn atoms) plus 16 PDI ligands was built from an initial guess in line with the experimental assumptions. The tetragonal lattice including 2 stacked layers of 4 units of $\{Zn_2(PDICl_4)_2\}$ (with a total of 1040 atoms) was optimized by relaxing both atomic positions and cell parameters without symmetry constraints but lattice angles fixed to 90°. A k-point sampling of 2×2×2 was used at the late stage of the optimization to secure the results. The final cell dimensions were a=56.11, b=56.10 and c=12.47 Å. The calculated unit cell is depicted in Figure S1 of the SI. Absorption properties of single molecules were calculated using time-dependent DFT with the range-separated hybrid functional CAM-B3LYP and the 6-311+G(d) Gaussian basis set. The absorption spectra of PDI dimers and trimers were computed with the same functional by using the smaller 6-311G(d) basis set. Calculations were performed using Gaussian16 package[18].

3. Results and discussion

The orange-coloured films of $\{Zn_2(PDICl_4)_2\}$ were grown at room temperature on ITO/glass substrates via spray-coating by liquid-phase epitaxy (LPE) in a layer-by-layer (LbL) fashion using zinc acetate as metal source and $PDICl_4$ as organic linker. Thanks to the low concentration of ligands, aggregation was not an issue and ethanol/DMF (95:5) solution could be used. The out-of-plane X-Ray Diffraction (XRD) data revealed highly oriented Zn-SurMOF-2 structure with [00*l*] orientation, which is consistent

with other SurMOFs obtained from various ditopic dicarboxylate linkers and zinc acetate via LPE methods[19,20]. The SurMOF structure consists of 2D square grid-like of $PDICl_4$ parallel and perpendicular to the surface, held together by a Zn paddle wheel (Figures 1a and 1b). These 2D sheets are then stacked in a AA fashion, as expected in a P*4* symmetric SurMOF-2 structure. The lattice dimension perpendicular to the substrate ($2\vartheta\ \lambda_{CuK\alpha}$ = 3.11°, a = 28 Å) closely matches with the length of the linker. Scanning Electron Microscopy (SEM) top-view pictures showed a flake-like morphology with a homogeneous coverage all over the ITO surface (Figure 1c). An optimized structure of the non-oriented parent MOF was obtained thanks to DFT. The presence of only [00*l*] planes on the experimental XRD confirms the oriented aspect of the SurMOF. In addition, the oriented structure was simulated and the resulting XRD pattern perfectly matches the experimental one (Figure 1d). The simulated structure revealed an inter-sheet distance of 6.2 Å, giving additional information over the SurMOF structure, since this distance could not be obtained experimentally because of the lack of dedicated instruments. Optimized unit cell parameters and other structural data are collected in the supporting information (Figure S1 and Table S1). In particular, the calculations revealed a significant distortion of the PDI aromatic cores, with an out-of-plane deviation of about 30° due to steric hindrance between chlorine atoms. Torsion angles ranging between 55° and 64° were also found between the PDI core and the lateral phenyl groups. The shortest distances between carbon atoms belonging to adjacent PDI units are equal to 3.3-3.4 Å, which indicates that the cohesion of the supramolecular architecture is ensured by a network of π-π interactions. Strong interlayer interactions between chlorine atoms and PDI cores are also evidenced, as shown by C-Cl distances in the 3.5-3.8 Å range. The stacking energy has been evaluated to 1.43 eV per $\{Zn_2(PDICl_4)_2\}$ unit.

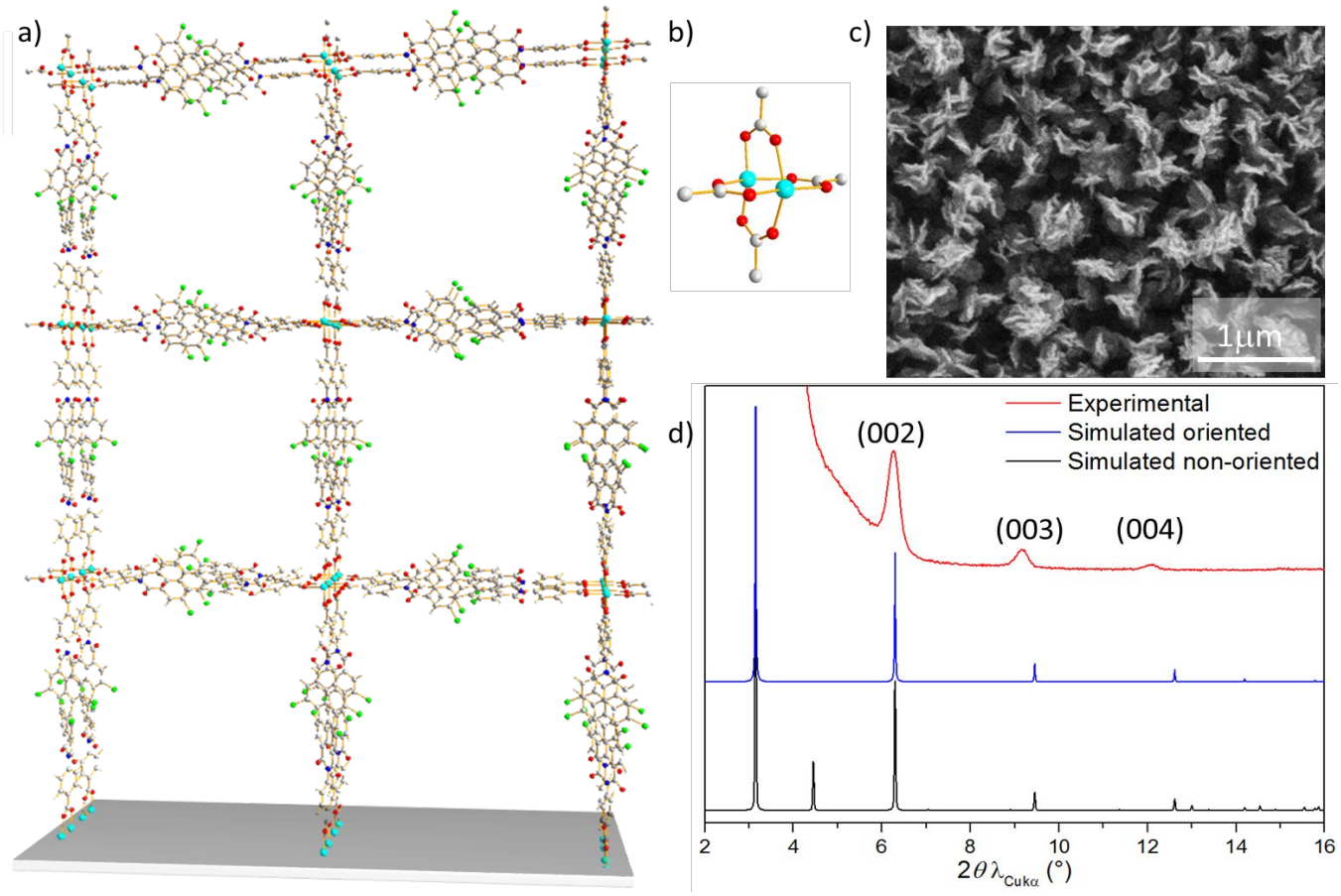

Figure 1. a) Simulated structure of $\{Zn_2(PDICl_4)_2\}$. b) Zn-paddlewheel isolated from the structure. (Colors for atoms: red = oxygen, grey = carbon, navy blue = nitrogen, green = chlorine, white = hydrogen and cyan = zinc). c) Top-view SEM picture. d) Simulated non-oriented (bottom), oriented (middle) and experimental (top) X-ray diffraction patterns.

In a previous article, in depth measurements in EMITFSI electrolyte were not given as a result of the lack of stability of the SurMOF in EMITFSI solution, mostly due to acidic protons located at the C2 position of the imidazolium, leading to the decohesion of the film from the substrate[9]. However, stability was greatly improved by using electrolyte with PMMA/butanone formulation, generating membranes rather than being liquid. This method implied the construction of prototype devices resulting from the assembly of SurMOF@ITO/glass films and ITO/glass slides through the electrolytic membrane (Figure 2a). The electrochemical and optical properties of the SurMOF were recorded in this configuration allowing additional information to be gathered in regards of the mechanism and the generation of different active species.

Because of the device configuration, reference electrodes cannot be used, hence reduction potentials obtained in solution with three electrodes cannot serve as reference[9].To assess the change in colour for the device, chronoamperometry (CA) was used in combination with absorption spectroscopy. Polarization of the device from 0.5 V to -4 V was performed for 150s followed each time by the recording of the full absorption spectrum from 1000 nm to 400 nm while applying the given potential. Between each polarization, CA at +0.5 V for 60s was applied to re-oxidize the SurMOF from its reduced cyan colour back to its original orange state (Figure 2b). In addition, such configuration may limit the EC performance as the counter electrode is not covered with an electrochemically active material.

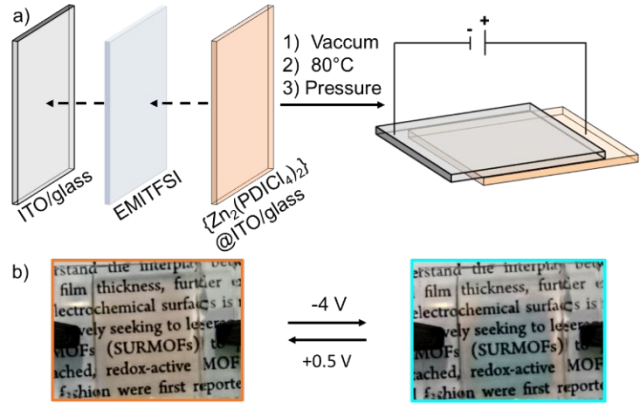

Figure 2. a) Scheme representation of the construction of the device. b) Picture of the colour switch of the device (glass/ITO/EMITFSI/{$Zn_2(PDICl_4)_2$}/ITO/glass).

Depending on the applied potential, different species were reversibly generated (Figure 3a). Reduction at -4 V led to the formation of a cyan species (λ_{max} = 680 nm) whereas reduction at -0.5 V generated an IR-absorbing species (λ_{max} = 770 nm, λ' = 925 nm). Thanks to their well-known spectroscopic signature[21] they were identified as the $PDICl_4$ radical dianions ($PDICl_4^{2-}$) and monoanions ($PDICl_4^{\cdot-}$), respectively (Figure 3b). Time-dependent (TD) DFT calculations performed on the isolated organic ligand in its crystalline geometry reproduced well the redshifts observed upon bi- and mono-reduction (Figure S3) and confirmed the assignment of the spectral bands. Furthermore, the absorption spectrum computed for the organic ligand connected on both sides to the metallic node did not show significant difference from that of the ligand alone, consistently with the localization of the frontier molecular orbitals on the organic core (Figure S4). This indicates that the optical properties of the SurMOF mainly arise from the organic units. However, a complete simulation of the device absorption spectrum would require inter-ligand interactions to be taken into account. Initial attempts in that direction have been made by simulating the spectra of PDI dimers and trimers extracted from the optimized crystal geometry, which show a slight blueshift of the main absorption band with the cluster size due to the H-aggregation of the organic chromophores (Figure S5).
In addition, the radical dianion has already been investigated by EPR in electrochromic SurMOF and the absorption spectra presented in this work is consistent with the one from this earlier study[9]. Interestingly, a state where both species coexist was generated while operating at -1 V. Interestingly, this potential yielded that state with the highest absorbance at 770 nm. In addition, the ratio of the two vibronic bands of the radical dianion is different compared to the full reduced state (-4 V), indicating that different absorbing species are involved in the reduction process. Further work should be dedicated to understand this behaviour, especially since inter-chromophoric interactions are expected in this kind of materials[19].
Chronoamperometry measurements highlighted two different processes depending on the species generated (Figure 3c). On one hand, a fast and clear return to the base line was observed while applying a potential of -0.5 V, indicating a fully finished process that takes place quite instantaneously. Interestingly, absorption spectroscopy showed the generation of $PDICl_4^{\cdot-}$ while the signal from the $PDICl_4$ initial state remains quite comparable to the as-deposited state, highlighting a possible equilibrium state where $PDICl_4$ and $PDICl_4^{\cdot-}$ coexist. This observation was also confirmed by quantum chemistry, highlighted by the presence of a band at 650 nm on the simulated absorption spectra of the mono-reduced ligand extracted from its crystalline state (Figure S2).
On the other hand, reduction at -4 V led to an unfinished process, highlighted by the remaining current after 150s. In addition, this final equilibrium state was achieved very slowly as indicated by the sluggish shape of the CA curve. In this case, spectroscopic contribution from $PDICl_4$ diminishes while the $PDICl_4^{2-}$ signal raises. The remaining of the $PDICl_4$ signal and the CA curve shape seem to indicate that complete transformation from $PDICl_4$ to $PDICl_4^{2-}$ could be pushed by applying more reductive conditions. However, due to ITO stability, a potential could not be applied beyond -4 V in the experimental configuration.

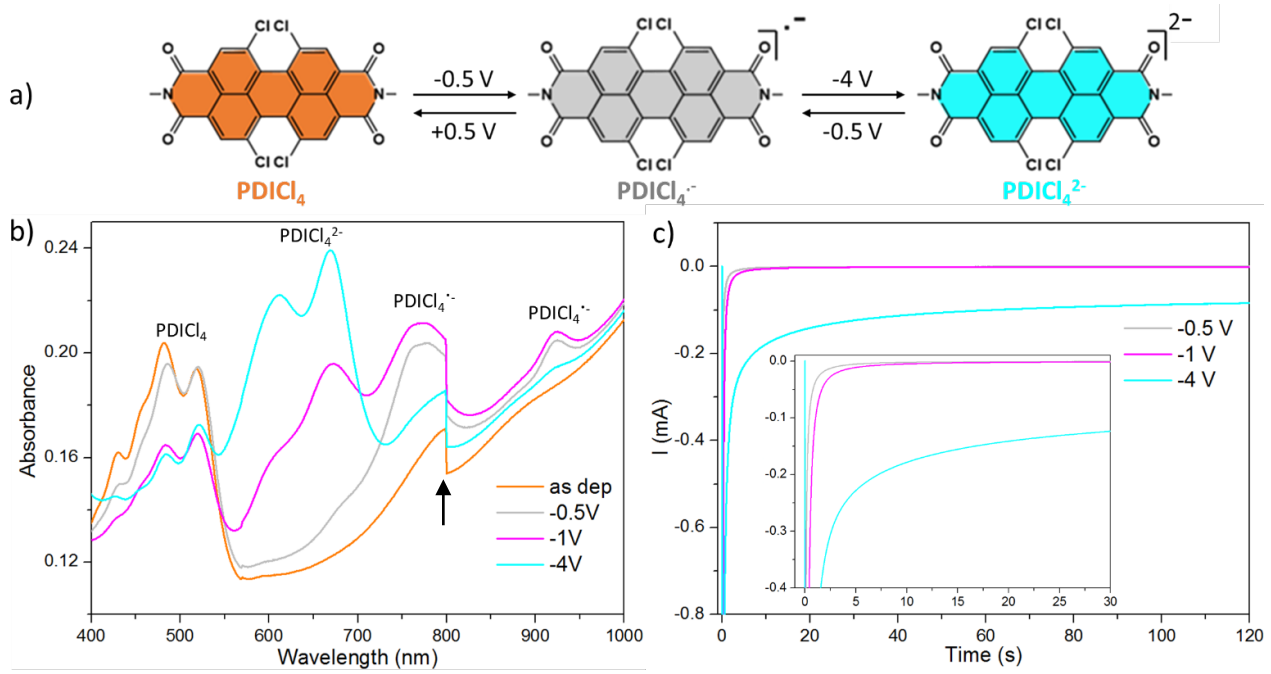

Figure 3. a) Illustration of the two-step reduction process of the $PDICl_4$ ligand. b) Absorption spectra of the as-deposited film and after polarization at -0.5, -1 and -4 V in EMITFSI. (Arrow: Abrupt drop at 800 nm originated from the measurement setup). c) Chrono-amperometry of the $\{Zn_2(PDICl_4)_2\}$ SurMOF with an inset of the first 30s.

4. Conclusions

To conclude, following a previously reported protocol, [00/] oriented electrochromic thin films were grown on ITO substrates at room temperature. The expected $\{Zn_2(PDICl_4)_2\}$ SurMOFs structure was simulated and optimized thanks to density functional theory. XRD patterns extracted from the computed structure perfectly matched the experimental data and thus confirmed the previously reported structure, highlighting the oriented aspect of the SurMOF. Furthermore, these calculations shed further light on the local environment of the ligand, the torsion angle of the $PDICl_4$ unit and the inter-sheet distance within the framework.

Quantum chemistry was also used to confirm the nature of the reduced states responsible for the electrochromic properties of the SurMOFs. These findings are fully consistent with the experimental data and confirmed the formation of $PDICl_4^{2-}$ upon reduction of the framework. The calculations also showed that the absorption properties of the neutral and reduced states are only dependent on the nature of the ligand core with no electronic contribution from the benzoic acid groups. These findings open a wider possibility of linker design for the building of electrochromic SurMOFs.

By using a device configuration consisting of a membrane-based electrolyte sandwiched between ITO/glass and the SurMOF thin films, electrochemical stability of the latter was greatly improved. Thanks to this configuration, in depth spectroelectrochemical characterizations were performed, revealing a two-step reduction process that was not observed using common electrochemical characterizations. Complete reduction was achieved by applying -4 V to the device, leading to a reversible colour change from the orange initial state to a cyan one attributed to the $PDICl_4$ dianions, as confirmed by the simulated absorption spectra of the bi-reduced $PDICl_4$ ligand extracted from the crystalline structure. In addition, a NIR absorbing state was generated and was attributed to the presence of the $PDICl_4$ mono-radical anion. Despite the remaining presence of the neutral $PDICl_4$, this species was generated with a very low potential and additional work should be dedicated to the complete mono-reduction as NIR electrochromic thin films may be of interest for smart windows applications.

Author Contributions

A.M. and A.R. conceived the idea and designed the experiments; A.M. carried out the SurMOFs syntheses and the material characterizations. F.C. and L.T. planned the theoretical calculations, F.C., L.T., M.F. and J.O carried out the theoretical calculations. A. M. prepared the manuscript with the inputs from all authors.

Conflicts of interest

The authors declare no conflict of interests.

Acknowledgements

This work was supported by the French National Research Agency (grant number ANR-20-CE29-0009-01) and by the Transnational Common Laboratory QuantumChemPhys (Theoretical Chemistry and Physics at the Quantum Scale, grant number ANR-10- IDEX-03-02) established between the

University of Bordeaux (UB), Euskal Herriko Unibertsitatea (UPV/EHU) and Donostia International Physics Center (DIPC). AM and AR acknowledge Dr. Fabrice Odobel and Dr. Stéphane Diring (University of Nantes) who provided the perylene diimide ligands and Dr. Nicolas Penin for his assistance for the implementation of the spray setup. AM and AR also thank Brandon Faceira and Alexandre Fargues for their help in optical measurements and 3D printing of the sample holder. Calculations were performed using the computing facilities provided by the "Mésocentre de Calcul Intensif Aquitain" (MCIA) of the Université de Bordeaux and the Université de Pauet des Pays de l'Adour.

Notes and references

1 C. G. Granqvist, *Solar Energy Materials and Solar Cells*, 2000, **60**, 201–262.

2 M. Stolar, 2020, **92**, 717–731.

3 P. M. Beaujuge and J. R. Reynolds, *Chem Rev*, 2010, **110**, 268–320.

4 X. Shao, Y. Yang, Q. Huang, D. Dai, H. Fu, G. Gong, C. Zhang, M. Ouyang, W. Li and Y. Dong, *Dalton Transactions*, 2023, **52**, 15440–15446.

5 C. R. Wade, M. Li and M. Dincă, *Angewandte Chemie - International Edition*, 2013, **52**, 13377–13381.

6 C. W. Kung, T. C. Wang, J. E. Mondloch, D. Fairen-Jimenez, D. M. Gardner, W. Bury, J. M. Klingsporn, J. C. Barnes, R. Van Duyne, J. F. Stoddart, M. R. Wasielewski, O. K. Farha and J. T. Hupp, *Chemistry of Materials*, 2013, **25**, 5012–5017.

7 R. A. Fischer and C. Wöll, *Angewandte Chemie - International Edition*, 2009, **48**, 6205–6208.

8 D. Zacher, O. Shekhah, C. Wöll and R. A. Fischer, *Chem Soc Rev*, 2009, **38**, 1418.

9 A. Mazel, L. Rocco, N. Penin and A. Rougier, *Adv Opt Mater*, 2023, **2**, 2202939.

10 H. Khandelwal, A. P. H. J. Schenning and M. G. Debije, *Adv Energy Mater*, 2017, **7**, 1602209.

11 R. Haldar, M. Jakoby, A. Mazel, Q. Zhang, A. Welle, T. Mohamed, P. Krolla, W. Wenzel, S. Diring, F. Odobel, B. S. Richards, I. A. Howard and C. Wöll, *Nat Commun*, 2018, **9**, 1–8.

12 R. Haldar, A. Mazel, M. Krstić, Q. Zhang, M. Jakoby, I. A. Howard, B. S. Richards, N. Jung, D. Jacquemin, S. Diring, W. Wenzel, F. Odobel and C. Wöll, *Nat Commun*, 2019, **10**, 1–7.

13 D R Bowler, T Miyazaki and M J Gillan, *Journal of Physics: Condensed Matter*, 2002, **14**, 2781.

14 T. Miyazaki, D. R. Bowler, R. Choudhury and M. J. Gillan, *J Chem Phys*, 2004, **121**, 6186–6194.

15 A. Nakata, J. S. Baker, S. Y. Mujahed, J. T. L. Poulton, S. Arapan, J. Lin, Z. Raza, S. Yadav, L. Truflandier, T. Miyazaki and D. R. Bowler, *J Chem Phys*, 2020, **152**, 164112.

16 D. R. Hamann, *Phys Rev B*, 2013, **88**, 85117.

17 D. R. Bowler, J. S. Baker, J. T. L. Poulton, S. Y. Mujahed, J. Lin, S. Yadav, Z. Raza and T. Miyazaki, *Jpn J Appl Phys*, 2019, **58**, 100503.

18 Gaussian 16, Revision B.01, Frisch, M.J., Trucks, G.W., Schlegel, H.B., Scuseria, G.E., Robb, M.A., Cheeseman, J.R.; Scalmani, G.; Barone, V.; Petersson, G.A.; Nakatsuji, H.; Li, X.; Caricato, M.; Marenich, A.V.; Bloino, J., Janesko, B.G., Gomperts, R., Mennucci, B., Hratchian, H.P., Ortiz, J.V., Izmaylov, A.F., Sonnenberg, J.L., Williams-Young, D., Ding, F., Lipparini, F., Egidi, F., Goings, J., Peng, B., Petrone, A., Henderson, T., Ranasinghe, D., Zakrzewski, V.G., Gao, J., Rega, N., Zheng, G., Liang, W., Hada, M., Ehara, M., Toyota, K., Fukuda, R., Hasegawa, J., Ishida, M., Nakajima, T., Honda, Y., Kitao, O., Nakai, H., Vreven, T., Throssell, K., Montgomery Jr., J.A., Peralta, J.E., Ogliaro, F., Bearpark, M.J., Heyd, J.J., Brothers, E.N., Kudin, K.N., Staroverov.

19 R. Haldar, A. Mazel, R. Joseph, M. Adams, I. A. Howard, B. S. Richards, M. Tsotsalas, E. Redel, S. Diring, F. Odobel and C. Wöll, *Chemistry - A European Journal*, 2017, **23**, 14316–14322.

20 J. Liu, B. Lukose, O. Shekhah, H. K. Arslan, P. Weidler, H. Gliemann, S. Bräse, S. Grosjean, A. Godt, X. Feng, K. Müllen, I. B. Magdau, T. Heine and C. Wöll, *Sci Rep*, 2012, **2**, 1–5.

21 V. Monnier, F. Odobel and S. Diring, *Chemical Communications*, 2022, 9429–9432.